Lab on a Chip

PAPER

View Article Online
View Journal | View Issue

Cite this: *Lab Chip*, 2025, **25**, 644

Synergistic binding ability of electrostatic tweezers and femtosecond laser-structured slippery surfaces enabling unusual droplet manipulation applications†

Xinlei Li, Chaowei Wang,* Zhenrui Chen, Cunyuan Chen, Suwan Zhu, Dong Wu and Jiale Yong*

Received 19th December 2024,
Accepted 22nd January 2025

DOI: 10.1039/d4lc01084a

rsc.li/loc

We propose a novel contactless droplet manipulation strategy that combines electrostatic tweezers (ESTs) with lubricated slippery surfaces. Electrostatic induction causes the droplet to experience an electrostatic force, allowing it to move with the horizontal shift of the EST. Because both the EST and the slippery operating platform prepared by a femtosecond laser exhibit a strong binding effect on droplets, the EST droplet manipulation features significant flexibility, high precision, and can work under various operating conditions. The EST can manipulate droplets with a wide volume range (500 nL–1 mL), droplets hanging on tilted or even inverted surfaces, multiple droplets in parallel, corrosive droplets, low-surface-tension organic droplets (*e.g.*, ethanol), and even droplets in a sealed space from the outside. The EST operation method is suitable for various slippery substrates prepared by femtosecond laser processing and can also be used to manipulate small solid spheres other than liquids. Additionally, a self-powered EST system is also designed without the need for high-voltage static electricity, allowing even fingers to serve as EST sources for droplet manipulation. The flexible and precise manipulation performance allows this technology to be applied in a variety of applications. For example, a new digital microfluidic (DMF) technology based on an EST array has been successfully validated and is expected to replace traditional electrowetting-on-dielectric technology in the future.

1. Introduction

Controllable droplet manipulation plays an important role in various liquid-related applications, such as microfluidics,[1,2] biological detection,[3,4] printing technology,[5,6] water collection,[7,8] chemical reactions,[9,10] energy conversion,[11,12] and thermal management.[13,14] In conventional contact-operation methods, droplets are easily contaminated by operating tools. Moreover, droplets may lose volume due to liquid adhesion, which reduces operational accuracy. In strict and high-end application scenarios, contactless droplet manipulation is urgently needed, where the operating tools do not directly touch the droplet.[15–17] Currently, several methods based on magnetic fields and light irradiation have been developed to achieve such contactless droplet manipulation.[18–23] However, since neither magnetic field nor light field can directly apply force to a droplet, these methods often rely on adding responsive additives to the substrate material and indirectly driving the droplet by modifying the surface topography or other physical and chemical properties of the operating platform.[18,21,22] Therefore, magnetic field-driven and light-driven methods are limited by the special material composition and surface morphology of the operating platform, which greatly restricts the application range of these intelligent droplet-manipulation technologies.

In daily life, static electricity can attract small objects, such as hair and scraps of paper. These phenomena raise the following question: can static electricity attract droplets and be used to move them? Researchers have reported that static electricity can directly exert a force on droplets.[24–26] To manipulate or transport a droplet, it is necessary not only to apply a driving force to the droplet but also to ensure that the operating platform has very low liquid adhesion to prevent droplet pinning. Superhydrophobic surfaces, such as lotus leaves, exhibit excellent water repellence, allowing water droplets to roll easily on such surfaces without adhering.[27,28]

CAS Key Laboratory of Mechanical Behavior and Design of Materials, Department of Precision Machinery and Precision Instrumentation, University of Science and Technology of China, Hefei, 230027, P. R. China. E-mail: chaoweiw@ustc.edu.cn, jlyong@ustc.edu.cn

† Electronic supplementary information (ESI) available: ESI is available from the author. See DOI: https://doi.org/10.1039/d4lc01084a

In recent years, novel noncontact manipulation methods for droplets have been developed in combination with electrostatic interactions and superhydrophobic platforms.[29–33] For example, Wang *et al.* successfully manipulated liquid droplets on a conductive superhydrophobic surface *via* a copper rod connected to high-voltage static electricity.[34] However, some inherent limitations of superhydrophobic surfaces make these methods of electrostatic droplet manipulation powerless in some special situations. For example, (a) droplets detach from a superhydrophobic surface when the surface is upright or overturned, making droplet manipulation impossible on inclined or overturned substrates.[35,36] (b) Despite their strong water repellence, superhydrophobic surfaces are easily wetted by organic liquids with low surface tension, rendering the superhydrophobic platform incapable of manipulating organic liquids *via* electrostatic interactions.[37]

The lubricated slippery structure of *Nepenthes* overcomes the abovementioned shortcomings of superhydrophobic materials.[38,39] Such slippery surfaces, also known as slippery liquid infused porous surfaces (SLIPS), resist liquid adhesion by filling porous surface microstructures with lubricant and forming a thin lubricant layer on the material's surface.[40] Droplets can slide easily on the slippery surfaces. Unlike superhydrophobic platform, SLIPS can hold droplets firmly in the vertical surface direction, while maintaining ultralow liquid adhesion in the parallel direction. During the sliding process, droplets cannot detach from the slippery surfaces,

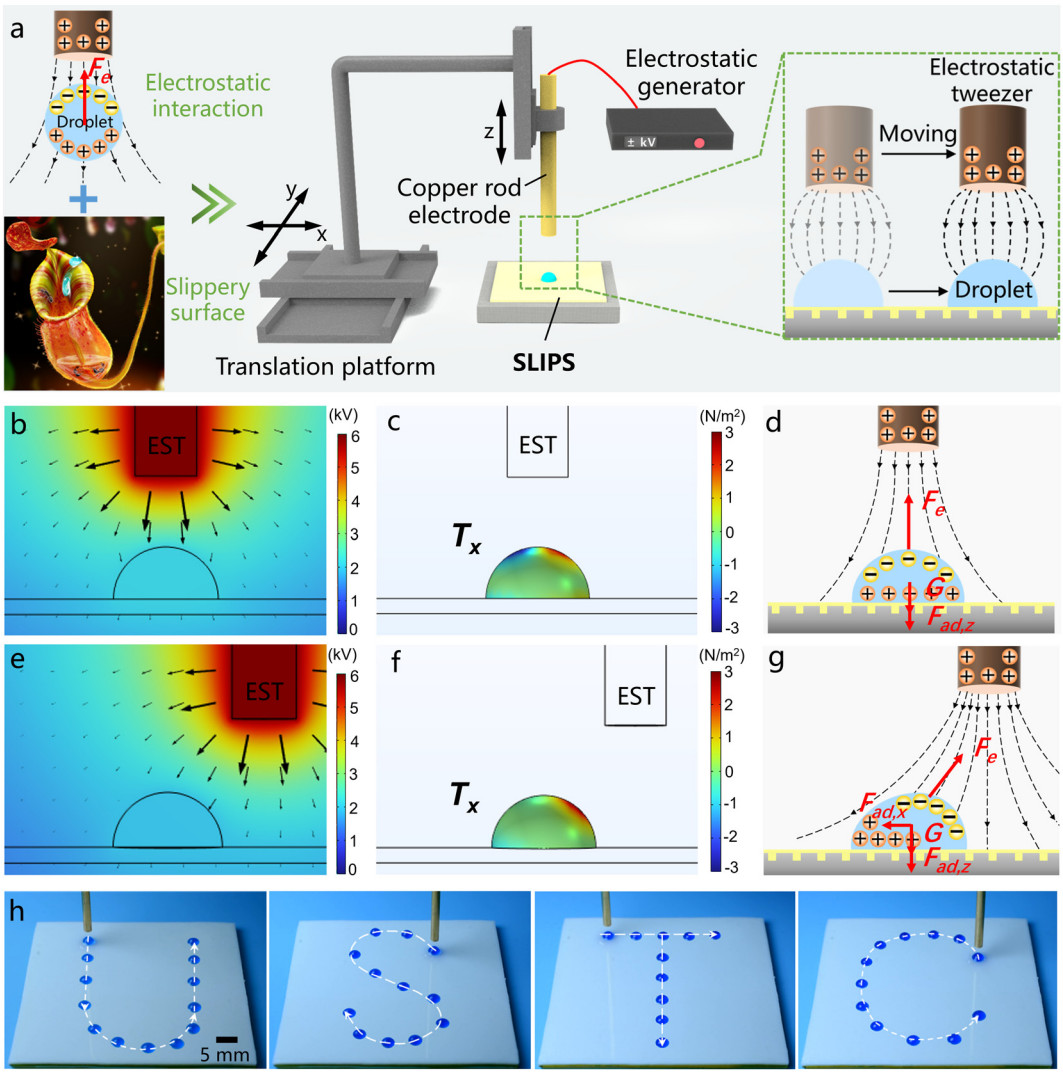

Fig. 1 System and mechanism of droplet manipulation by combining electrostatic interactions and lubricated slippery surfaces (*i.e.*, SLIPS). (a) The designed system for droplet manipulation: design idea (left), operating system (middle), and operating method (right). The image of *Nepenthes* is used from ref. 39 with permission. (b–g) Simulation and force analysis showing the mechanism of EST droplet manipulation: (b and e) distribution of the electrostatic potential and electric field intensity (the arrows reflecting its local direction and strength) around a +6 kV charged rod electrode, (c and f) distribution of the horizontal component (T_x) of the Maxwell stress tensor acting on the surface of the droplet, and (d and g) force analysis of the droplets under electrostatic interaction. The droplets in (b–d) are directly under the EST, and the droplets in (e–g) horizontally deviate from the EST. The black dotted lines with arrows in (a, d and g) indicate the electric field lines. (h) Stacked images of using an EST to guide a 10 μL droplet to move along the designed trajectory of the letters "USTC".

whether the substrates are upright or overturned. On the other hand, owing to the unique antiliquid principle, SLIPS can repel a broad range of liquids, including organic liquids, making it possible to manipulate organic liquids with low surface tension through electrostatic action.[40]

Here, we propose a new strategy for contactless droplet manipulation by combining electrostatic tweezers (ESTs) with lubricated slippery surfaces, as shown in Fig. 1a. On the basis of electrostatic interactions, the EST can easily manipulate droplets on a femtosecond laser-structured slippery surface. In particular, when the slippery platform is tilted or turned upside down, droplets hanging on the surface can still be transported effectively. A variety of liquids can be manipulated, including common daily liquids, corrosive acid/alkali/salt solutions, and even organic liquids (such as ethanol droplets with extremely low surface tension). Additionally, a self-powered EST system is also proposed, enabling the manipulation of droplets without the need for high-voltage input. As proof-of-concept examples, several representative applications based on EST droplet manipulation are successfully demonstrated.

2. Results and discussion

2.1 System of EST droplet manipulation

Fig. 1a (middle) shows a schematic diagram of the EST device for droplet manipulation. The EST system is mainly composed of a copper rod electrode, an electrostatic generator, and a slippery operating platform. The copper rod electrode is fixed vertically to a three-dimensional (3D) mobile system and positioned above the droplet that is previously placed on a lubricated slippery platform. The bottom end of the copper rod is kept at an appropriate height from the droplet. The upper end of the rod is connected to an electrostatic generator that supplies high-voltage static electricity to the copper electrode. The charged rod electrode can exert an attractive effect on the droplet. When the EST is shifted horizontally by the mobile system, the droplet on the slippery operating platform will move with it (right inserted schematic in Fig. 1a).

2.2 Mechanism of droplet manipulation by EST

Fig. 1b–g reveals the physical mechanism by which the EST is able to manipulate droplets on SLIPS. The charged rod electrode creates an electrostatic field in the surrounding space. In general, the electrostatic potential and field intensity decrease with increasing distance from the charged electrode (Fig. 1b and e). The droplet in this electrostatic field undergoes electrostatic induction, resulting in the redistribution of the internal positive and negative charges.[41,42] Taking the positive potential of the EST as an example, the negative charge inside the droplet migrates to the surface near the EST, while the positive charge migrates to the far side (Fig. 1d and g). This nonuniform distribution of positive/negative charges leads to the electrical polarity of the droplet, causing it to experience an electrostatic force ($\boldsymbol{F}_e$) in the electrostatic field. The electrostatic-induced polarization charge, q, on an area unit of the surface of the droplet is:[30,42]

$$q = (\varepsilon - 1)\varepsilon_0|\nabla \boldsymbol{E}| \quad (1)$$

where ε is the dielectric constant of the liquid, ε_0 is the dielectric constant of air, and $\boldsymbol{E} = -\nabla V$ (V is the spatial electric potential) is the vector of the electric field. According to Coulomb's law, the net electrostatic force on this area unit of the droplet surface can be expressed as follows:[24,43,44]

$$\boldsymbol{F}_e = \boldsymbol{E}q = (\varepsilon - 1)\varepsilon_0|\nabla \boldsymbol{E}|\boldsymbol{E} \quad (2)$$

The electrostatic force on the entire droplet is the sum of the Maxwell stress acting on the whole surface of the droplet and can be calculated as an integral of the surface area (S):[34,45,46]

$$\boldsymbol{F}_e = \oint\left[\varepsilon \boldsymbol{E}(\boldsymbol{E}\boldsymbol{n}) - \frac{\varepsilon}{2}\boldsymbol{E}^2\boldsymbol{n}\right]\mathrm{d}S \quad (3)$$

where $\boldsymbol{n}$ is the unit normal. Combined with the Maxwell stress tensor ($\boldsymbol{T}_e$) acting on the droplet, $\boldsymbol{F}_e$ can be quantified in tensor form as:[47,48]

$$\boldsymbol{F}_e = \oint \boldsymbol{T}_e \cdot \boldsymbol{n}\mathrm{d}S, \text{ with } \boldsymbol{T}_{e,ij} = \varepsilon_0\left(\boldsymbol{E}_i\boldsymbol{E}_j - \frac{\delta_{ij}}{2}\boldsymbol{E}^2\right),\ i, j = x, y, z \quad (4)$$

where δ_{ij} is the Kronecker function. The distribution of $\boldsymbol{T}_e$ can be calculated *via* COMSOL-Multiphysics simulation, reflecting the forces acting on different units of the droplet surface, as shown in Fig. 1c and f.

When the droplet is directly under the EST, the distribution of the electric field on both sides of the droplet is symmetrical (Fig. 1b). The horizontal components of $\boldsymbol{T}_e$ on both sides are equal in value but opposite in direction (Fig. 1c). Therefore, the resultant $\boldsymbol{F}_e$ in the horizontal direction is zero (Fig. 1d). When the EST moves forward, the droplet deviates from the position directly below the EST, resulting in a horizontal deviation distance between the droplet and the EST. The electric field is no longer symmetrical (Fig. 1e). In particular, its intensity at the surface of the droplet near the EST is greater than that on the other side, making the attractive effect of the EST on the near surface of the droplet stronger than the repulsive effect on the far side (Fig. 1f). The droplet is attracted by the EST as a whole, and the horizontal component of the $\boldsymbol{F}_e$ points toward the position of the EST, as shown in Fig. 1g. In another case, when a negative potential is applied to the EST, the droplet can also be attracted (Fig. S1, ESI†). Since the slippery operating platform has ultralow adhesion to the droplets along the surface, the horizontal adhesion force ($F_{ad,x}$) of the droplet on such a surface is very small. Therefore, the high value of $\boldsymbol{F}_e$ is sufficient to overcome $F_{ad,x}$ and drive the droplet toward the EST ($\boldsymbol{F}_e\cos\theta > F_{ad,x}$, where θ is the angle between the $\boldsymbol{F}_e$ and the operating platform), resulting in the droplet eventually returning to the position directly below the

EST. Under electrostatic interactions, droplets will always remain under the EST and be trapped by the charged EST. In contrast, due to the slippery surface has a high adhesion force ($F_{ad,z}$) on the liquid droplet in the vertical surface direction, the vertical component of F_e cannot easily overcome the gravity (G) of the droplet and the adhesion force of the platform to the droplet in the vertical direction ($F_e \sin\theta < F_{ad,z} + G$). This characteristic ensures that the liquid droplet always stays on the slippery platform.

Since the droplets follow the EST, we can easily move them on lubricated slippery platforms by shifting the EST horizontally. The sliding process of droplets on a silicone oil-lubricated surface is also affected by motion resistance, mainly arising from viscous forces ($F_\mu \sim \pi\gamma_{wo}R\mathrm{Ca}^{2/3}$, where γ_{wo} is the interfacial energy between water and oil, R is the radius of the droplet, $\mathrm{Ca} = \mu_0 v/\gamma_{wo}$ is the capillary number, μ_0 is the viscosity of the silicone oil used, and v is the droplet sliding velocity).[49,50] Therefore, on the basis of Newton's law of motion, the droplet motion can be described as:

$$F_e \cos\theta - F_\mu = M\frac{dv}{dt} \quad (5)$$

where M and t are the mass of the droplet and time, respectively. It can be seen that the viscosity of the lubricant

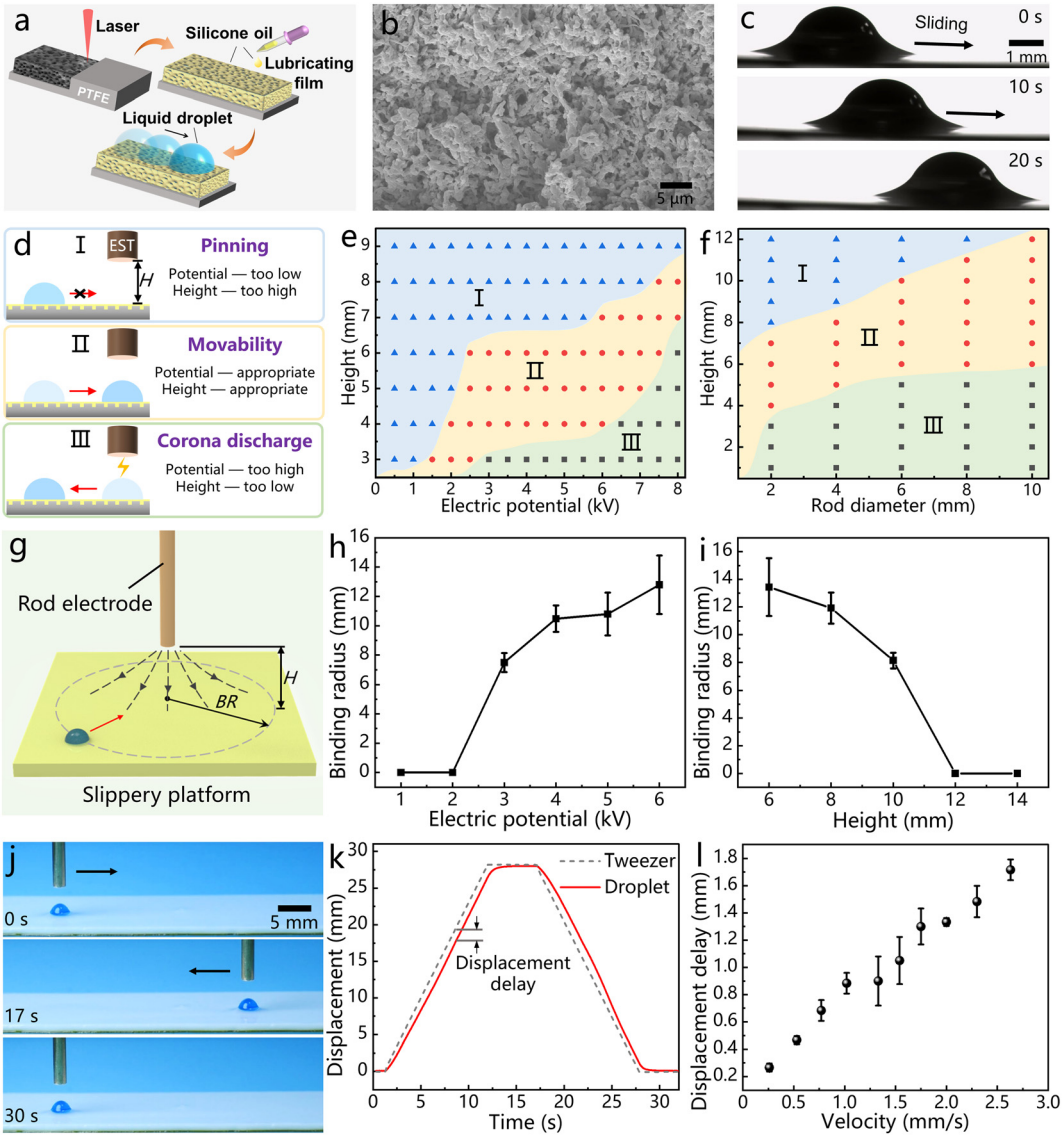

Fig. 2 EST-based droplet manipulation. (a) Preparation process of lubricated slippery surfaces by femtosecond laser treatment. (b) Morphology of the laser-induced porous microstructure on the PTFE surface. (c) Sliding process of a water droplet on the slippery surface with a tilt angle of 2°. (d) Schematic of three situations for droplet manipulation. (e) Phase map showing the influences of the electric potential and height of the EST on the droplet manipulation process (rod diameter = 2 mm). (f) Influence of the diameter of the copper rod on droplet manipulation (electrostatic potential = +6 kV). (g) Definition of the binding radius (BR). (h and i) Influence of (h) the electrostatic potential (at a height of 6 mm) and (i) the height (at a potential of +6 kV) of the EST on the binding radius. (j) A cycle of moving a droplet forward and back with an EST. (k) Displacement changes of the EST and the droplet over time in the process of (j). (l) Relationship between the displacement delay and the operating velocity.

will affect the speed of droplet operation. In the preparation of a SLIPS, it is necessary to select a low-viscosity lubricant (*e.g.*, 10 cSt silicone oil in our experiment) to ensure that the speed of EST droplet manipulation is not too low. As the position of the EST is flexibly controlled by a mechanical moving system, the EST can manipulate droplets to transport along any designed path on the lubricated slippery operating platform. For example, Fig. 1h and Movie S1 (ESI†) show the process of using an EST to guide a water droplet along the complex trajectory of the letters "USTC", demonstrating the high operational accuracy and flexibility of the EST operation.

2.3 Factors affecting droplet manipulation

The preparation of the *Nepenthes*-inspired SLIPS involved femtosecond laser processing with subsequent lubrication infusion, as shown in Fig. 2a.[39] First, the surface of the hydrophobic polytetrafluoroethylene (PTFE) sheet was ablated by a femtosecond laser (Fig. S2, ESI†),[51–53] resulting in the formation of porous rough microstructures on the PTFE surface (Fig. 2b and S3 in the ESI†). Then, electrically insulating silicone oil was used as a lubricating fluid to infuse into the laser-induced porous microstructures. After removing excess silicone oil, a thin lubricant layer was trapped on the PTFE surface. The as-prepared lubricated slippery surface exhibits excellent repulsive capacity for various liquids (Fig. S4 and Movie S2, ESI†) because the captured lubricant layer can effectively block contact between the liquids and the PTFE surface (Fig. S5, ESI†). Liquid droplets can slide down easily on this slippery surface (Fig. 2c). As long as the lubricated slippery surface is tilted to 1°, the water droplets on it can easily slide down, albeit slowly. The sliding velocity of the droplet increases with the increase of the tilt angle of the substrate (Fig. S6, ESI†).

The electric potential and height of the EST have important effects on the droplet manipulation process. According to eqn (3), the larger the electric potential or the lower the height of the EST, the greater the attraction of the droplet. In general, there are three states for droplet manipulation on the as-prepared slippery platform using an EST, as shown in Fig. 2d. When the electric potential of the EST is too low or the height is too high (state-I), the small electrostatic force on the droplet is insufficient to drive its motion, causing the droplet to remain in place regardless of how the EST is moved horizontally. When the EST has an appropriate potential and height (state-II), allowing the droplet to follow the EST's motion effectively. However, when the electric potential is too high and the height of the EST is too low (state-III), the droplet will be charged *via* the disruptive discharge process and repelled laterally.[41,54] Fig. 2e shows the influence of the electric potential and height of the EST on droplet manipulation. Only ESTs with an appropriate electrostatic potential and maintaining an appropriate height can effectively move the droplet. Additionally, the diameter of the rod electrode used also affects electrostatic droplet manipulation, as shown in Fig. 2f. Under the same electrostatic potential conditions, the appropriate operating height required by the charged rods with different diameters is also different, mainly because the electric field intensity generated by different charged rods in space is different.

Only droplets that deviate within a limited horizontal distance from the EST can be pulled back by electrostatic forces. Beyond this critical distance, droplets will not be trapped by the EST. This critical distance is defined as the binding radius (BR), as shown in Fig. 2g, which reflects the binding strength of the EST on the droplet. A larger BR indicates that the EST has a higher control strength over the droplet. Fig. 2h and i show the effects of the electrostatic potential and height of the EST on the BR. The BR increases with increasing electrostatic potential and decreases with increasing height of the EST. The results indicate that within a suitable range, an EST with a higher electrostatic potential and lower height has a stronger binding ability on the droplets, mainly because this EST generates a greater electric field intensity in space.

Fig. 2j and Movie S3 (ESI†) show the process of manipulating a droplet forward and then back with an EST. The corresponding position changes of the EST and the droplet over time are depicted in Fig. 2k. There is a position hysteresis of the droplet relative to the EST during the motion, caused by the viscous resistance of the droplet on the slippery surface (eqn (5)). This displacement delay increases with increasing operating velocity (Fig. 2l). Although there is a small hysteresis in the droplet movement, when the EST stopped, the droplet eventually reaches the position directly below the EST, showing high operating accuracy (Fig. 2k and Movie S3†).

2.4 Multifunctional droplet manipulation

The EST can directly apply electrostatic force to droplets. Its strong trapping ability, combined with the special characteristics of the lubricated slippery platform, allows it to achieve a wide range of droplet-manipulation functions. For example, the EST can manipulate liquids across a broad volume spectrum. Droplets as small as 500 nL (Fig. 3a) and as large as 1 mL (Fig. 3b) can be driven, as shown in Movie S4 (ESI†). The strong controlling ability enables the EST to drive the droplet to overcome gravity and climb an inclined slippery surface (Fig. 3c and Movie S4†). Because of the high droplet adhesion of the slippery surfaces in the vertical surface direction, droplets on these surfaces will not fall off, even when the surfaces are turned over. Therefore, the manipulation of droplets suspended on an overturned surface is allowed (Fig. 3d and Movie S4†). Such operations cannot be performed on a superhydrophobic platform, as droplets will detach from the superhydrophobic surface. Additionally, an EST array can be used to manipulate multiple droplets simultaneously, achieving parallel droplet manipulation (Fig. 3e and Movie S4†).

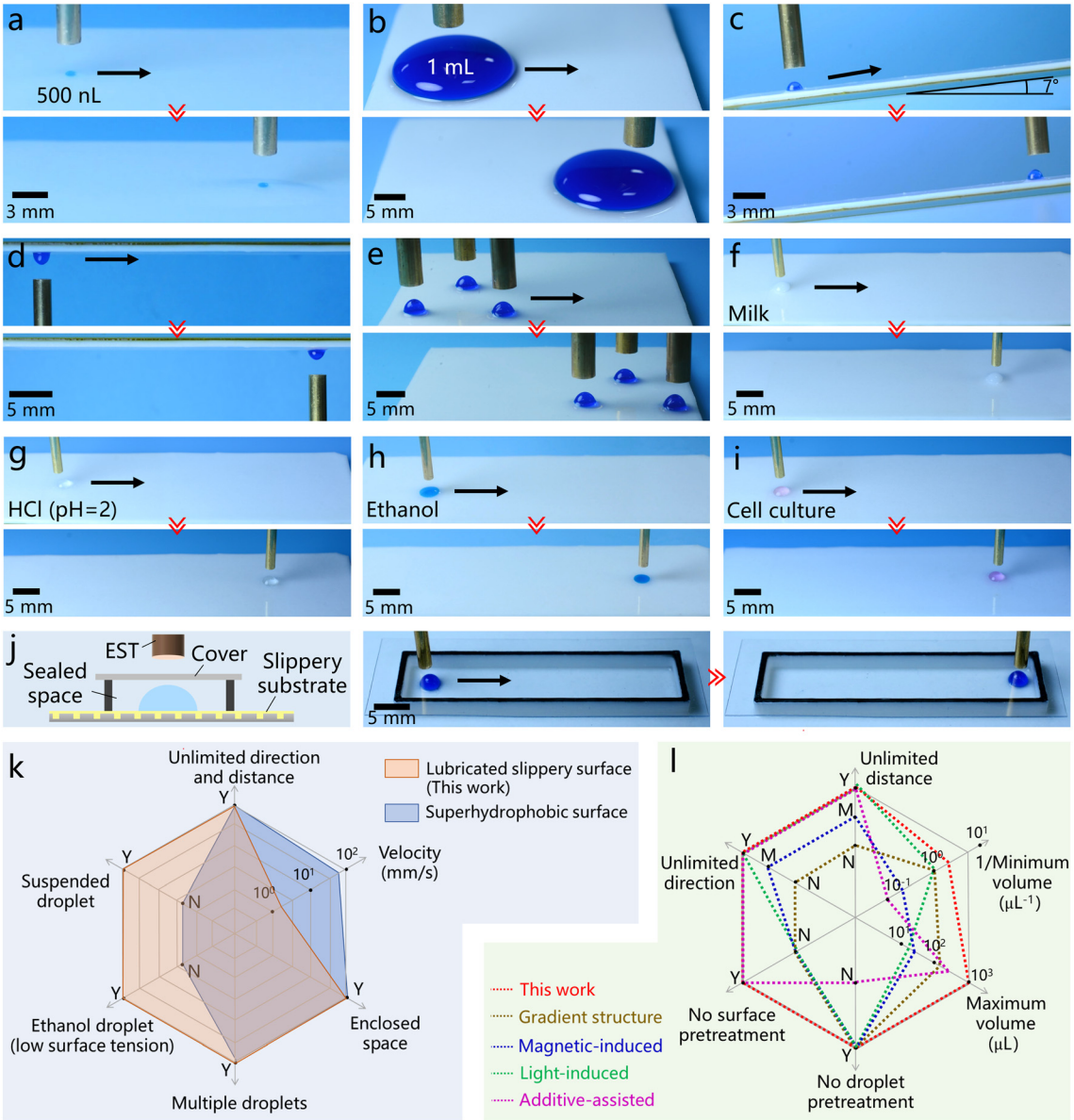

Fig. 3 Multifunctional droplet manipulation *via* EST. (a and b) Manipulating droplets with different volumes: (a) 500 nL and (b) 1 mL. (c) Driving a droplet to slide upward along the 7° inclined slippery surface. (d) Moving a droplet hanging on an overturned surface. (e) Parallel manipulation of multiple droplets by an EST array. (f–i) Manipulation of different kinds of liquids: (f) milk droplets in daily life, (g) corrosive HCl acid droplets with pH = 2, (h) organic ethanol droplets (surface tension = 22.3 mN m^{-1}), and (i) cell-culture medium droplets. (j) Externally manipulating a droplet sealed in an enclosed space from the outside. (k) Comparison of the EST for manipulating droplets on a lubricated slippery platform and on a superhydrophobic platform.[34] (l) Performance comparison between the EST and other representative methods (*e.g.*, gradient structures,[55] magnetic field-driven methods,[56] light-driven methods,[57] and additive-assisted methods[58]) for droplet manipulation on slippery substrates from six aspects. "Y", "M", and "N" denote "yes", "medium", and "no", respectively.

As a special kind of superwetting surface, SLIPS can repel various liquids. Common daily liquids, such as milk, coffee, cola, and juice, can be easily moved by an EST on the slippery operating platform (Fig. 3f and S7 and Movie S5 in the ESI†). In general, the lubricated slippery surface has excellent corrosion resistance because the infused lubricant completely prevents the corrosive liquids from directly touching the base material. This property enables the manipulation of corrosive liquids (Movie S6, ESI†), such as strong HCl acid droplets with pH = 2 (Fig. 3g), strong NaOH alkali droplets (Fig. S8a, ESI†), and 10% NaCl salt droplets (Fig. S8b, ESI†). In contrast to superhydrophobic surfaces, which mainly repel water, lubricated slippery surfaces can also repel organic liquids with low surface tension, enabling the use of an EST to manipulate various organic droplets. Fig. 3h and Movie S7 (ESI†) show the transport of an ethanol droplet with a surface tension as low as 22.3 mN m^{-1}. In particular, organic solvents such as cell culture liquid can be remotely manipulated in a noncontact manner, laying the foundation for the use of ESTs in biomedical applications (Fig. 3i and Movie S7†). In

contrast, ethanol droplets and cell culture droplets usually wet superhydrophobic surfaces directly, which prevents organic droplets from being manipulated on superhydrophobic platforms.

Femtosecond lasers have the ability to process any given material and can construct rough porous microstructures on a wide range of material surfaces.[51] Therefore, the lubricated slippery surfaces can be easily prepared on a variety of substrates by combining femtosecond laser treatment and subsequent infusion of lubrication fluids. For example, Fig. S9 and Movie S8 (ESI†) show the processes of using an EST to operate droplets on the as-prepared slippery aluminum metal, glass, and silicon surfaces. It is indicated that the lubricated slippery surfaces prepared by femtosecond laser processing make the EST droplet manipulation method suitable for various material substrates. On the other hand, solid matter can also respond to the surrounding electrostatic field. Thus, in addition to liquid droplets, EST can also manipulate small solid spheres on the laser-structured surfaces, such as small plastic spheres, glass beads, and stainless steel balls (Fig. S10 and Movie S9, ESI†). To avoid the adhesion of the liquid layer to the solid balls, the structured substrate does not need to be filled with lubricating liquid (*e.g.*, silicone oil) for solid manipulation.

Electrostatic fields have the ability to penetrate electrically insulating materials, allowing the EST to operate liquids through electrically insulating materials, *e.g.*, droplets in a confined space can be manipulated from outside. As shown in Fig. 3j, a water droplet is sealed in an enclosed space consisting of a slippery substrate, a rectangular enclosure, and an insulating polydimethylsiloxane (PDMS) top cover. The EST can apply an electrostatic force to the droplet inside the system from the outside, enabling the droplet to be moved on demand without opening the closed system (Movie S10, ESI†). This external control of internal technology has great potential in many special application scenarios, especially when these application systems cannot be opened or are not allowed to be opened.

Fig. 3k compares the advantages and disadvantages of the EST for manipulating droplets on a lubricated slippery platform *versus* on a superhydrophobic platform. Although the operating velocity on slippery surfaces is lower than that on superhydrophobic surfaces, the ability to manipulate liquid droplets on inclined or even inverted surfaces and the ability to manipulate various organic liquids (even ethanol) with low surface tension on slippery platforms are not available for EST on superhydrophobic platforms.[34] Fig. 3l compares the EST with other reported methods for droplet manipulation on slippery substrates. The EST shows advantages in terms of its universal adaptability to surfaces and droplets and its strong manipulation ability. For example, droplet motion driven by gradient structures usually has an unchangeable transport direction along the gradient direction and a limited travel distance.[15,55,59–61] Droplet transport driven by a magnetic field or light irradiation requires surface pretreatments, such as the addition of responsive additives to the substrate and the preparation of pillar-like surface microstructures.[9,18–23,56,57] Manipulation by additives requires the pre-addition of external field-controlled additives inside the droplets.[58,62,63] In contrast, ESTs can flexibly guide droplet to move in any direction without direction or distance restrictions. By directly applying force to the droplet, the EST can perform droplet manipulation on ordinary slippery surfaces without pretreating the substrates and droplets. Moreover, the ability to apply electrostatic force directly to the droplets gives the EST strong flexibility and high precision in terms of droplet manipulation. In particular, the strong trapping force on droplets allows the EST to manipulate ultralarge droplets and ultrasmall droplets more effectively.

2.5 Self-powered EST droplet manipulation

The ESTs described above require an electrostatic generator to apply high-voltage static electricity to a metal electrode. However, many droplet manipulation requirements are temporary, or there may be no electrostatic generator equipment around when the droplets need to be operated. Here, we also propose a simple self-powered EST strategy that can realize the droplet operation functions without the need for electrostatic generators. As shown in Fig. 4a, the surface of a plastic plate (*e.g.*, polymethyl methacrylate (PMMA)) is triboelectrically charged by a simple friction process, giving its surface a certain electrostatic potential in advance. The as-prepared SLIPS is then placed on the charged plate, and a liquid droplet is placed on it. Horizontal transport of the droplet can be achieved by moving an ordinary metal rod (without connecting to an electrostatic generator) horizontally above the droplet. As shown in Fig. 4b–e, the charged plastic plate generates an electrostatic field in space. When a conductive copper rod is inserted in this electric field, it changes the distribution of the spatial electric field. When the metal rod is directly above the droplet, the electric field is symmetrically distributed relative to the droplet center (Fig. 4b). The electrostatic forces acting on the droplet from the left and right are symmetric (Fig. 4c). Once the metal rod moves forward, the droplet will horizontally deviate from the rod. At this time, the electrostatic field around the droplet center is no longer symmetrical (Fig. 4d). The horizontal electrostatic force on the droplet toward the metal rod is greater than that in the opposite direction, resulting in a net force that drive the droplet to the position underneath the metal rod (Fig. 4e). Therefore, the droplet can be transported freely by the inserted conductive rod, mainly because that the rod breaks the symmetry of the electrostatic field generated by the charged substrate. In this manner, droplet manipulation can be performed without the input of high-voltage static electricity. Fig. 4f and Movie S11 (ESI†) show the process of moving a water droplet forward and backward through a copper rod. This self-powered EST still maintains high manipulation accuracy (Fig. 4g). In addition to metals, other conductive materials can also serve as EST sources for

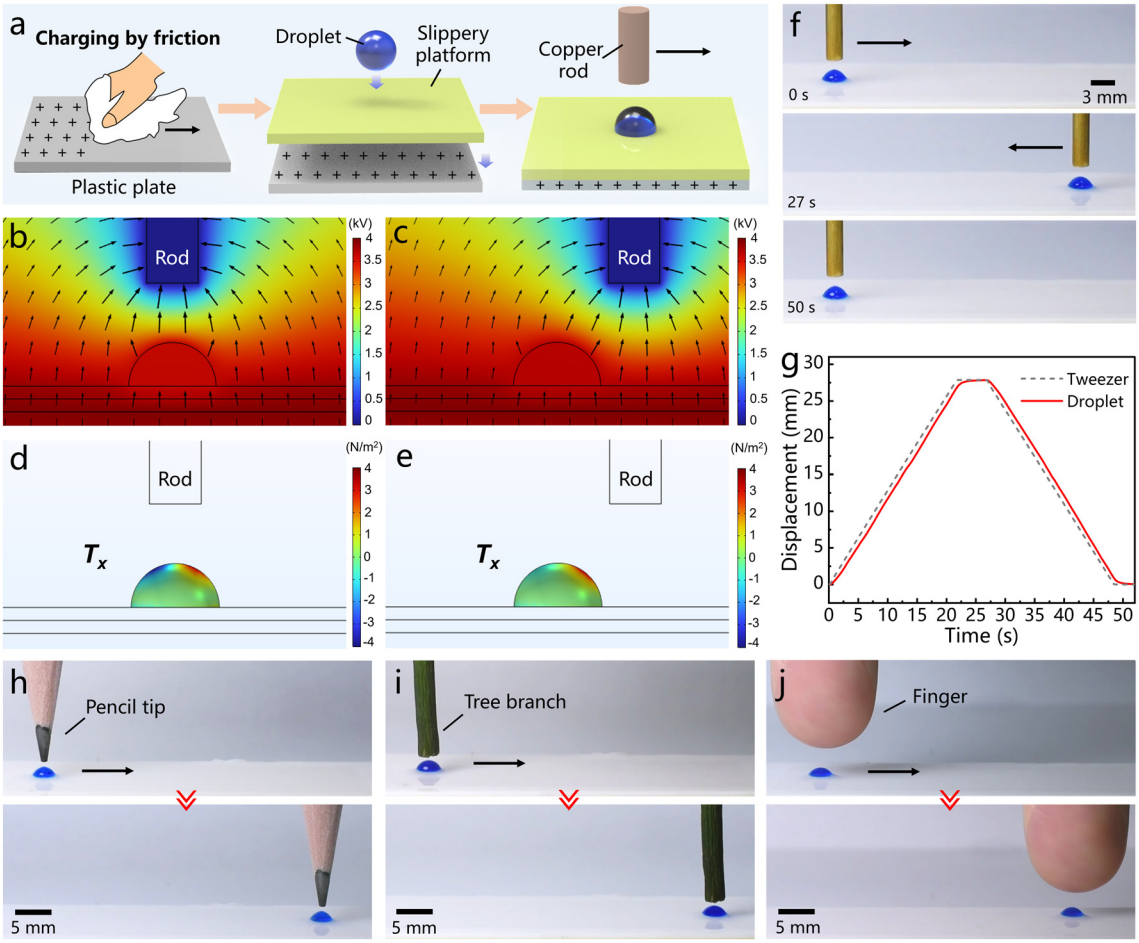

Fig. 4 Self-powered EST for electrostatic droplet manipulation without the use of an electrostatic generator. (a) Schematic of the designed system. A plastic plate is triboelectrically charged by a simple friction process in advance and the charged plate is used as the substrate; the slippery PTFE sheet is then placed on the charged substrate; and, liquid droplets are dropped onto the slippery surface. (b–g) Simulation analysis showing the physical mechanism of self-powered EST droplet manipulation: (b and c) distribution of the electrostatic potential and electric field intensity (the arrows) generated by a +4 kV charged substrate, (d and e) distribution of the horizontal component (T_x) of the Maxwell stress tensor applied to the droplet. (f) Process of moving a water droplet forward and then backward with a copper rod. (g) Displacement changes of the droplet and the copper rod over time in (f). (h–j) Processes of using conductive (h) pencil tips, (i) fresh tree branches, and even (j) fingers to guide the transport of liquid droplets.

droplet manipulation. For example, pencil tips (Fig. 4h), fresh tree branches (Fig. 4i), and even fingers (Fig. 4j) can guide the transport of liquid droplets in this self-powered system (Movie S11†).

2.6 Various applications of EST droplet manipulation

The strong binding ability of the EST to droplets, along with its flexible and precise manipulation performance, allow this technology to be used in a variety of applications. For example, an EST can guide different droplets to contact and merge. When droplets serve as carriers of chemical reagents, droplet coalescence enables trace interactions between different chemicals, also known as droplet microreactions. As shown in Fig. 5a and Movie S12 (ESI†), a phenol droplet is guided by an EST to contact an $FeCl_3$ droplet. The combined droplet quickly turns purple due to a color microreaction ($6C_6H_5OH + Fe^{3+} \rightarrow [Fe(C_6H_5O)_6]^{3-} + 6H^+$). When the merged droplet is further moved to contact another $AgNO_3$ droplet, a white precipitate ($Cl^- + Ag^+ \rightarrow AgCl\downarrow$) generates inside the droplet. Organic chemical microreactions are possible because the slippery operating platforms allow the EST to manipulate various organic droplets. In contrast, organic microreactions are usually not feasible on superhydrophobic platforms because organic droplets can wet the superhydrophobic surface and thus cannot be moved.

The electrical circuit can be connected by operating conductive droplets. We simulate a disconnected circuit system and attempt to connect the circuit using a conductive droplet controlled by an EST. As shown in Fig. 5b, a conductive NaCl droplet is guided to the broken location of the circuit and thus touches the two ports of the broken circuit. The LED lamp in the circuit system is then lit, indicating that the circuit is successfully connected (Fig. 5c and Movie S13 in the ESI†). This method can not only be used to connect circuits but also serve as a switch to control

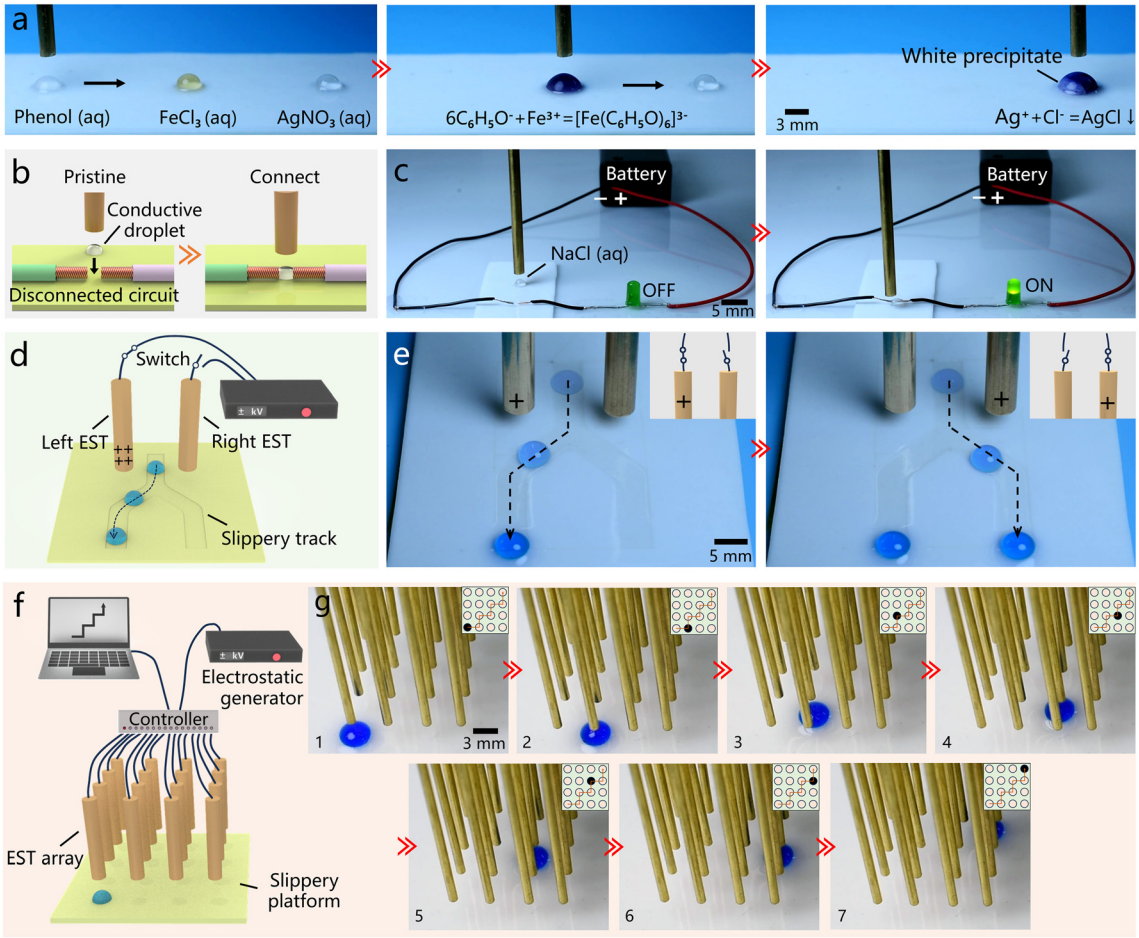

Fig. 5 Diverse applications based on EST droplet manipulation. (a) Droplet microreactions. An organic phenol droplet was guided by an EST to contact an $FeCl_3$ droplet and further contact an $AgNO_3$ droplet. (b) Schematic drawing and (c) experimental result of connecting a disconnected electrical circuit *via* EST droplet manipulation. A conductive NaCl droplet was transported to connect the two ports of a broken circuit. (d) Schematic drawing and (e) experimental presentation of the designed electrostatic-induced trajectory switching system. The insets show the connection state of the two electrodes on the left and right. By selectively connecting the left or right EST, the sliding droplets were selectively transported along different channels of an inverted Y-shaped slippery track. (f) Schematic of the proposed EST-based digital microfluidic chip. (g) Experimental function verification of the designed EST-based DMF: by controlling the digital signal of each EST, droplet transport occurs along the set trajectory. The insets in (g) depict the connection condition of each electrode of the EST array (solid ring: "1", connected with electrostatic power; hollow ring: "0", disconnected with electrostatic power).

circuit's on and off states, and it can even be used to repair damaged circuit systems.

In microfluidics, it is usually necessary to selectively guide liquids or droplets to transport along different channels, especially at forks. The attraction of the EST to droplets is expected to switch the motion trajectory of droplets in the open-channel microfluidic system. As a proof of concept, we designed an electrostatic-induced trajectory switching system, as shown in Fig. 5d. An inverted Y-shaped slippery concave track is prepared on the surface of a PTFE sheet *via* femtosecond laser etching. The platform is tilted slightly, allowing droplets to slide down the track under gravity. Two ESTs are placed above each side of the fork. By selectively connecting one EST to the electrostatic generator, the sliding droplet can be deflected toward that side due to electrostatic attraction (Fig. S11, ESI†). For example, as shown in Fig. 5e and Movie S14 (ESI†), when the EST on the left is charged, the droplets slide down the track on the left; when the EST on the right side is charged, the droplets slide down the track on the right side. The electrostatic switch features a short response time and facile operation.

Digital microfluidics (DMF), a new automatic control technology for full-range discrete droplets, is an innovation of traditional microfluidics.[64,65] Currently, DMF is mainly achieved *via* electrowetting-on-dielectric (EWOD) technology, usually with the aid of a complex embedded control circuit. Flexible and precise droplet manipulation by EST provides a simpler alternative method for realizing DMF. As shown in Fig. 5f, we design a proof-of-concept DMF chip based on an EST array and a slippery platform. An array of 4 × 4 ESTs is positioned vertically above the slippery platform at a suitable height. The ESTs are separately connected to the controller which is linked to an electrostatic generator. Through the control software, the controller manages the on–off state of each EST through digital signals (*i.e.*, "1" and "0"). When static electricity is applied to one EST, the droplet on the

lubricated slippery platform moves to the selected location directly below this EST due to electrostatic attraction. Once this EST is disconnected and then another nearest neighboring EST is charged, the droplet moves further to the position below the newly charged EST. By controlling the digital signal of each EST, the movement path of droplets can be precisely designed and controlled, allowing droplet to transport along the set trajectory in a programmable manner, as shown in Fig. 5g and Movie S15 (ESI†). In contrast to classical EWOD, there is no direct electrical contact between the voltage source and the droplet for the EST-based DMF.

2.7 Comparison of the current EST technology and traditional electrostatic droplet manipulation

Although Li *et al.* have previously applied static electricity to a glass rod with a diameter of 7 mm by a friction process and successfully used the triboelectric charged rod to manipulate droplets on a slippery platform, such an operation is a rough way of droplet manipulation in terms of operating accuracy and controllability.[66] Firstly, the electrically insulated glass rod obtains electrostatic charges through friction process. The strength of the generated electrostatic potential is random through friction; that is, it is difficult to accurately control the potential of the electrostatic rod. An appropriate potential value close to the target can only be obtained by repeated friction. Secondly, the electrostatic potential of the charged rod is not stable, and it will gradually decline when the charged rod is exposed to the air. Thirdly, the diameter of the used glass rod is relatively large, which will affect the accuracy of the droplet operations. In contrast, the current EST technology with using an electrostatic generator to provide high-voltage static electricity to the copper electrode can avoid the abovementioned problems. The potential of the EST can be continuously adjusted *via* the electrostatic generator. Moreover, the EST can remain stable electric potential for a long time. The use of copper electrodes makes the potential of the EST and the spatial electric field distribution more uniform. As a result, the proposed EST method can realize many functions and applications that cannot be realized by the traditional triboelectric charged rod.[66] For example, in the applications of microfluidics and digital microfluidics shown in Fig. 5d and f, the electrodes need to be constantly and repeatedly switched between the charged (connected) and deenergized (disconnected) states. Such an operation is easy to achieve with the current EST method, but almost impossible with conventional electrostatic droplet manipulation based on triboelectric charged rods.

3. Conclusions

In conclusion, we have developed a multifunctional droplet manipulation strategy by combining ESTs with lubricated slippery platforms. Due to electrostatic induction, droplets on slippery platform are subjected to an electrostatic force and can move with the horizontal shift of the EST. Because both the EST and the slippery operating platform exert strong binding forces on the droplet, this EST-based manipulation method exhibits characteristics of strong flexibility and high precision, and can operate under a wide range of conditions. The EST can manipulate droplets with a broad volume range (500 nL–1 mL), droplets hanging on tilted or even inverted surfaces, multiple droplets simultaneously (in parallel), various common daily liquids, corrosive droplets, low-surface-tension organic droplets (such as ethanol with a surface tension as low as 22.3 mN m^{-1}), and even droplets in sealed spaces from the outside. The EST operation method can be extended to various slippery substrates (such as metal, glass, and silicon sheets) prepared by femtosecond laser processing and can also be used to manipulate small solid spheres (such as plastic spheres, glass beads, and stainless steel balls) other than liquids. A self-powered EST system without high-voltage input is also proposed, and even fingers can be used as EST sources to flexibly manipulate droplets. The flexible and precise manipulation performance allows this technology to be used in a variety of applications, such as chemical microreactions, connecting/repairing electrical circuits, and electrostatic-induced liquid trajectory switching systems. In particular, the use of an EST array enables a simpler strategy to achieve DMF function compared to traditional EWOD technology.

EST droplet manipulations on lubricated slippery surfaces and superhydrophobic surfaces are two complementary ways. Both ways have their own advantages, but also have their own shortcomings. In different application scenarios, it is necessary to select an appropriate operating platform (superhydrophobic surface or SLIPS) according to the requirements. Under specific requirements (*e.g.*, manipulating organic liquids or operating liquids on inclined surfaces), EST shows an advantage in controlling droplets on a lubricated slippery platform compared to those on a superhydrophobic platform. It is also demonstrated that the combination of an EST and a slippery platform has significant advantages over previously reported representative droplet-manipulation methods in many aspects, especially in terms of universal adaptability to surfaces and droplets and strong manipulation capabilities.

4. Experimental section

4.1 Preparation of the lubricated slippery platform

PTFE sheets (thickness = 1 mm) were utilized as substrates, and femtosecond laser ablation was used to produce rough porous microstructures on the PTFE surface. The laser beam (pulse duration = 75 fs, repetition rate = 1 kHz, wavelength = 800 nm) from a laser system (Spectra-Physics, USA) was focused on the PTFE sheet through an s-9210d galvanometer scanner (Sunny Technology, China) and an f–θ lens (focal length = 16 cm). A laser power of 300 mW, a scanning speed of 10 mm s^{-1}, and a scanning space of 20 μm were adopted in the line-by-line laser scanning process. The low-viscosity silicone oil (10 cSt, PMX-200) was chosen as the lubricant in

order to allow the liquid droplets to slide more easily on the as-prepared slippery surface and thus ensure the speed of EST manipulation. The structured PTFE sheets were cleaned and immersed in silicone oil for 20 minutes, allowing silicone oil to infuse the laser-induced porous microstructures. Then, the PTFE sheets were removed from the silicone oil and placed upright for 10 minutes to remove excess lubricant. As a result, an ultrathin layer of trapped lubricant with a thickness of ~50 μm formed on the PTFE surface, resulting in a lubricated slippery surface. Similarly, the lubricated slippery aluminum, glass, and silicon surfaces were prepared by femtosecond laser processing, fluorosilane modification, and the infusion of silicone oil.

4.2 EST droplet manipulation

The EST system is mainly composed of a copper rod electrode, a lubricated slippery PTFE sheet, and an electrostatic generator. The laser-structured slippery PTFE sheet was used as the operating platform, and liquid droplets were placed on this sheet. The copper rod with diameter ranging from 2 to 10 mm was fixed on a 3D mobile platform and was located directly above the droplet. The upper end of the copper rod was connected to an electrostatic generator (DW-P303-1ACH2, Dong Wen, China) with an input voltage of AC220V and an output power of ≤30 W. By horizontally moving the charged copper rod, the droplet followed the designed EST and was transported on the slippery PTFE platform.

4.3 Self-powered EST droplet manipulation

The surface of a PMMA plate (thickness = 3 mm) was positively charged by rubbing the filter paper. Then, the as-prepared slippery PTFE sheet was placed on the charged PMMA plate, and the liquid droplet was released onto the slippery surface. Metal rods, pencil tips, fresh tree branches, and even fingers were used as EST sources. They were placed vertically above the droplet and maintained at an appropriate height from the droplet. When those ESTs were horizontally shifted, the droplet was transported with them on the slippery platform.

4.4 Electrostatic simulation

The distributions of the generated electrostatic potential and electric field were calculated *via* COMSOL Multiphysics software (MA, USA). The electrostatic field physics module was used. The parameters used were the same as those used in the experiment.

4.5 Characterization

A GeminiSEM 500 scanning electron microscope (Carl Zeiss, German) was used to observe the laser-induced microstructure on the PTFE surface. The contact angle and sliding process of the droplets on the PTFE surface were measured by a homemade contact-angle measuring instrument. The processes of droplet manipulation were recorded through a D7100 digital camera (Nikon, Japan).

Data availability

The data that support the findings of this study are available from the corresponding author upon reasonable request.

Author contributions

D. W. supervised the project. J. Y. proposed the research idea, conceived the project, and written the manuscript. X. L. performed the main experiments. All the authors contributed to the analysis, manuscript writing and editing.

Conflicts of interest

There are no conflicts to declare.

Acknowledgements

This work was supported by the National Key Research and Development Program of China (No. 2024YFB4610700), the National Natural Science Foundation of China (No. 62475251 and 62325507), and the USTC Research Funds of the Double First-Class Initiative (No. YD2090002013). We acknowledge the Experimental Center of Engineering and Material Sciences at USTC for the fabrication and measurement of the samples. This work was partly carried out at the USTC Center for Micro- and Nanoscale Research and Fabrication and at the USTC Instruments Center for Physical Science.

References

1 M. Abdelgawad and A. R. Wheeler, *Adv. Mater.*, 2009, **21**, 920–925.
2 R. Seemann, M. Brinkmann, T. Pfohl and S. Herminghaus, *Rep. Prog. Phys.*, 2011, **75**, 016601.
3 J. Song, W. Cheng, M. Nie, X. He, W. Nam, J. Cheng and W. Zhou, *ACS Nano*, 2020, **14**, 9521–9531.
4 I. Hajji, M. Serra, L. Geremie, I. Ferrante, R. Renault, J.-L. Viovy, S. Descroix and D. Ferraro, *Sens. Actuators, B*, 2020, **303**, 127171.
5 V. Jokinen, L. Sainiemi and S. Franssila, *Adv. Mater.*, 2008, **20**, 3453–3456.
6 Z. Dong, J. Ma and L. Jiang, *ACS Nano*, 2013, **7**, 10371–10379.
7 Y. Zheng, H. Bai, Z. Huang, X. Tian, F.-Q. Nie, Y. Zhao, J. Zhai and L. Jiang, *Nature*, 2010, **463**, 640–643.
8 S. Zhang, J. Huang, Z. Chen and Y. Lai, *Small*, 2017, **13**, 1602992.
9 G. Cheng, C. Y. Kuan, K. W. Lou and Y.-P. Ho, *Adv. Mater.*, 2024, **36**, 2313935.
10 D. Wu, Z. Zhang, Y. Zhang, Y. Jiao, S. Jiang, H. Wu, C. Li, C. Zhang, J. Li, Y. Hu, G. Li, J. Chu and L. Jiang, *Adv. Mater.*, 2020, **32**, 2005039.
11 Y. Wang, S. Guo, W. Xu and Z. Wang, *Adv. Funct. Mater.*, 2020, **30**, 1908252.

12 A. Li, H. Li, S. Lyu, Z. Zhao, L. Xue, Z. Li, K. Li, M. Li, C. Sun and Y. Song, *Nat. Commun.*, 2023, **14**, 2646.
13 M. Jiang, Y. Wang, F. Liu, H. Du, Y. Li, H. Zhang, S. To, S. Wang, C. Pan, J. Yu, D. Quéré and Z. Wang, *Nature*, 2022, **601**, 568–572.
14 Z. Cheng, C. Wang, X. Li, T. Xu, Z. Chen, Z. Cui, K. Cheng, S. Zhu, D. Wu and J. Yong, *Appl. Phys. Lett.*, 2024, **124**, 061601.
15 C. Yang, Q. Zeng, J. Huang and Z. Guo, *Adv. Colloid Interface Sci.*, 2022, **306**, 102724.
16 J. Xu, S. Xiu, Z. Lian, H. Yu and J. Cao, *Droplet*, 2022, **1**, 11–37.
17 Z. Yuan, C. Lu, C. Liu, X. Bai, L. Zhao, S. Feng and Y. Liu, *Sci. Adv.*, 2023, **9**, eadg2352.
18 S. Jiang, D. Wu, J. Li, J. Chu and Y. Hu, *Droplet*, 2024, **3**, e117.
19 J. Wang, Z. Zhu, P. Liu, S. Yi, L. Peng, Z. Yang, X. Tian and L. Jiang, *Adv. Sci.*, 2021, **8**, 2103182.
20 S. Jiang, Y. Hu, H. Wu, R. Li, Y. Zhang, C. Chen, C. Xue, B. Xu, W. Zhu, J. Li, D. Wu and J. Chu, *Nano Lett.*, 2020, **20**, 7519–7529.
21 F. Wang, M. Liu, C. Liu, T. Wang, Z. Wang and X. Du, *Sci. Adv.*, 2022, **8**, eabp9369.
22 W. Li, X. Tang and L. Wang, *Sci. Adv.*, 2020, **6**, eabc1693.
23 S. Tan, X. Han, Y. Sun, P. Guo, X. Sun, Z. Chai, L. Jiang and L. Heng, *ACS Nano*, 2024, **18**, 8484–8495.
24 Y. Jin, C. Wu, P. Sun, M. Wang, M. Cui, C. Zhang and Z. Wang, *Droplet*, 2022, **1**, 92–109.
25 J. G. Kim, D. J. Im, Y. M. Jung and I. S. Kang, *J. Colloid Interface Sci.*, 2007, **310**, 599–606.
26 N. Li, L. Wu, C. Yu, H. Dai, T. Wang, Z. Dong and L. Jiang, *Adv. Mater.*, 2018, **30**, 1703838.
27 L. Feng, S. Li, Y. Li, H. Li, L. Zhang, J. Zhai, Y. Song, B. Liu, L. Jiang and D. Zhu, *Adv. Mater.*, 2002, **14**, 1857–1860.
28 J. Yong, F. Chen, Y. Fang, J. Huo, Q. Yang, J. Zhang, H. Bian and X. Hou, *ACS Appl. Mater. Interfaces*, 2017, **9**, 39863–39871.
29 H. Dai, C. Gao, J. Sun, C. Li, N. Li, L. Wu, Z. Dong and L. Jiang, *Adv. Mater.*, 2019, **31**, 1905449.
30 Q. Sun, D. Wang, Y. Li, J. Zhang, S. Ye, J. Cui, L. Chen, Z. Wang, H.-J. Butt, D. Vollmer and X. Deng, *Nat. Mater.*, 2019, **18**, 936–941.
31 X. Han, R. Jin, Y. Sun, K. Han, P. Che, X. Wang, P. Guo, S. Tan, X. Sun, H. Dai, Z. Dong, L. Heng and L. Jiang, *Adv. Mater.*, 2024, **36**, 2311729.
32 J. Nie, Z. Ren, J. Shao, C. Deng, L. Xu, X. Chen, M. Li and Z. L. Wang, *ACS Nano*, 2018, **12**, 1491–1499.
33 X. Tang and L. Wang, *ACS Nano*, 2018, **12**, 8994–9004.
34 Y. Jin, W. Xu, H. Zhang, R. Li, J. Sun, S. Yang, M. Liu, H. Mao and Z. Wang, *Proc. Natl. Acad. Sci. U. S. A.*, 2022, **119**, e2105459119.
35 S. Pan, A. K. Kota, J. M. Mabry and A. Tuteja, *J. Am. Chem. Soc.*, 2013, **135**, 578–581.
36 J. Yong, Y. Fang, F. Chen, J. Huo, Q. Yang, H. Bian, G. Du and X. Hou, *Appl. Surf. Sci.*, 2016, **389**, 1148–1155.
37 J. Yong, F. Chen, Q. Yang, J. Huo and X. Hou, *Chem. Soc. Rev.*, 2017, **46**, 4168–4217.
38 T. S. Wong, S. H. Kang, S. K. Tang, E. J. Smythe, B. D. Hatton, A. Grinthal and J. Aizenberg, *Nature*, 2011, **477**, 443–447.
39 J. Yong, J. Huo, Q. Yang, F. Chen, Y. Fang, X. Wu, L. Liu, X. Lu, J. Zhang and X. Hou, *Adv. Mater. Interfaces*, 2018, **5**, 1701479.
40 M. Villegas, Y. Zhang, N. Abu Jarad, L. Soleymani and T. F. Didar, *ACS Nano*, 2019, **13**, 8517–8536.
41 W. D. Ristenpart, J. C. Bird, A. Belmonte, F. Dollar and H. A. Stone, *Nature*, 2009, **461**, 377–380.
42 X. Han, S. Tan, R. Jin, L. Jiang and L. Heng, *J. Am. Chem. Soc.*, 2023, **145**, 6420–6427.
43 J. Yong, X. Li, Y. Hu, Y. Peng, Z. Cheng, T. Xu, C. Wang and D. Wu, *Int. J. Extreme Manuf.*, 2024, **6**, 035002.
44 F. Wang, Y. Sun, G. Zong, W. Liang, B. Yang, F. Guo, C. Yangou, Y. Wang and Z. Zhang, *ACS Appl. Mater. Interfaces*, 2022, **14**, 3526–3535.
45 D. R. Link, E. Grasland-Mongrain, A. Duri, F. Sarrazin, Z. Cheng, G. Cristobal, M. Marquez and D. A. Weitz, *Angew. Chem., Int. Ed.*, 2006, **45**, 2556–2560.
46 F. Wang, F. Guo, Z. Wang, H. He, Y. Sun, W. Liang and B. Yang, *Langmuir*, 2022, **38**, 13697–13706.
47 W. Xu, Y. Jin, W. Li, Y. Song, S. Guo, B. Zhang, L. Wang, M. Cui, X. Yan and Z. Wang, *Sci. Adv.*, 2022, **8**, eade2085.
48 Y. Jin, X. Liu, W. Xu, P. Sun, S. Huang, S. Yang, X. Yang, Q. Wang, R. H. W. Lam, R. Li and Z. Wang, *ACS Nano*, 2023, **17**, 10713–10720.
49 D. Daniel, J. V. I. Timonen, R. Li, S. J. Velling and J. Aizenberg, *Nat. Phys.*, 2017, **13**, 1020–1025.
50 A. Keiser, P. Baumli, D. Vollmer and D. Quéré, *Phys. Rev. Fluids*, 2020, **5**, 014005.
51 J. Yong, Q. Yang, X. Hou and F. Chen, *Ultrafast Sci.*, 2022, **2022**, 9895418.
52 Y. Zhang, Y. Jiao, C. Li, C. Chen, J. Li, Y. Hu, D. Wu and J. Chu, *Int. J. Extreme Manuf.*, 2020, **2**, 032002.
53 J. Yong, Q. Yang, J. Huo, X. Hou and F. Chen, *Int. J. Extreme Manuf.*, 2022, **4**, 015002.
54 Q. Tang, X. Liu, X. Cui, Z. Su, H. Zheng, J. Tang and S. W. Joo, *Langmuir*, 2021, **37**, 14697–14702.
55 M. Soltani and K. Golovin, *Adv. Funct. Mater.*, 2022, **32**, 2107465.
56 K. Shao, S. Jiang, Y. Hu, Y. Zhang, Y. Zhang, J. Li, D. Wu and J. Chu, *Adv. Funct. Mater.*, 2022, **32**, 2205831.
57 S. Zhou, J. Yang, R. Li, Y. Chen, C. Li, C. Chen, Y. Tao, S. Fan, D. Wu, L. Wen, B. Qiu and W. Ding, *Nano Lett.*, 2023, **23**, 10710–10718.
58 A. Li, H. Li, Z. Li, Z. Zhao, K. Li, M. Li and Y. Song, *Sci. Adv.*, 2020, **6**, eaay5808.
59 C. Zhang, L. Wang, C. R. Crick and Y. Lu, *Prog. Mater. Sci.*, 2025, **147**, 101358.
60 X. Zhang, S. Ben, Z. Zhao, Y. Ning, Q. Li, Z. Long, C. Yu, K. Liu and L. Jiang, *Adv. Funct. Mater.*, 2023, **33**, 2212217.

61 X. Xiao, C. Zhang, H. Ma, Y. Zhang, G. Liu, M. Cao, C. Yu and L. Jiang, *ACS Nano*, 2019, **13**, 4083–4090.
62 Y. Zhang, S. Jiang, Y. Hu, T. Wu, Y. Zhang, H. Li, A. Li, Y. Zhang, H. Wu, Y. Ding, E. Li, J. Li, D. Wu, Y. Song and J. Chu, *Nano Lett.*, 2022, **22**, 2923–2933.
63 Y. He, K. Yin, L. Wang, T. Wu, Q. Deng, Y. Dou and C. J. Arnusch, *Nano Lett.*, 2023, **23**, 4947–4955.
64 K. Choil, A. H. C. Ng, R. Fobel and A. R. Wheeler, *Annu. Rev. Anal. Chem.*, 2012, **5**, 413–440.
65 S. P. Zhang, J. Lata, C. Chen, J. Mai, F. Guo, Z. Tian, L. Ren, Z. Mao, P.-H. Huang, P. Li, S. Tang and T. J. Huang, *Nat. Commun.*, 2018, **9**, 2928.
66 X. Li, C. Wang, Y. Hu, Z. Cheng, T. Xu, Z. Chen, J. Yong and D. Wu, *ACS Appl. Mater. Interfaces*, 2024, **16**, 18154–18163.

